Archives of Hydro-Engineering and Environmental Mechanics
Vol. 53 (2006), No. 2, pp. 105–126

Loads Exerted on a Cylindrical Structure by Floating Ice Modelled as a Viscous-Plastic Material

Ryszard Staroszczyk

Institute of Hydro-Engineering of the Polish Academy of Sciences,
Waryńskiego 17, 71-310 Szczecin, Poland, e-mail: rstar@ibwpan.gda.pl

(Received September 27, 2005; revised May 15, 2006)

Abstract

In this paper the problem of interaction between a coherent floating ice field and a fixed, rigid, vertically-walled circular cylinder is investigated. The ice cover, of horizontal dimensions significantly larger than the characteristic size of the structure, is assumed to be driven against the cylinder by wind drag forces. The ice is treated as a viscous-plastic material, in which the permissible stress states in the horizontal plane are bound by an elliptic yield curve. By using an associated flow rule, a constitutive law, involving two parameters defining the ice strength in compression and much smaller strength in extension, is derived in order to describe the behaviour of the material. The law predicts distinct responses during yield (occurring at high strain-rates) and during the flow when the yield condition does not apply (at lower strain-rates). The results of numerical calculations performed by a finite difference method illustrate, for chosen ice rheological parameters, the distribution of contact stresses at the ice – structure interface. Two forms of boundary conditions at the cylinder wall, free-slip and no-slip, are considered, and their effects on the horizontal loads sustained by the structure are examined. In addition, the results for the viscous-plastic rheology of ice are compared with those obtained on the assumption of a purely viscous behaviour of ice.

Key words: floating ice, cylindrical structure, rheology, viscosity, plasticity

Notations

C_a, C_w	–	wind and water drag coefficients,
$D_{rr}, D_{\theta\theta}, D_{r\theta}$	–	strain-rate components,
$\mathbf{D}$	–	strain-rate tensor,
e	–	dimensional rheological parameter,
h	–	ice sheet thickness,
$\mathbf{I}$	–	unit tensor,
N_r, N_θ	–	axial internal forces per unit width of an ice sheet,
$N_{r\theta}$	–	shear internal force per unit width of an ice sheet,
q_r, q_θ	–	distributed load intensities,
p	–	mean pressure in ice,

P_1, P_2 – ice strength parameters,
r, θ, z – cylindrical polar coordinates,
R_0 – cylinder radius,
v_r, v_θ – horizontal ice velocity components,
γ, η – strain-rate invariants,
ζ, ζ_m – bulk viscosities of ice,
Δ, Δ_c – strain-rate invariants,
μ, μ_m – shear viscosities of ice,
ϱ_a, ϱ_w – air and water densities,
$\sigma_{rr}, \sigma_{\theta\theta}, \sigma_{r\theta}$ – stress components,
$\boldsymbol{\sigma}$ – stress tensor.

1. Introduction

Although the problem of determination of forces which floating ice exerts on off-shore structures is important for the assessment of the safety and reliability of the latter, there is still no general agreement among researchers and engineers as to the most proper rheological model that should be applied in order to describe the behaviour of ice. During short-time ice – structure interaction events, lasting from seconds to minutes, an obvious choice is to assume elastic or viscoelastic behaviour of the ice, and disregard from the analysis any creep or plastic deformations in the material. On the other hand, during the long-term events, in extreme cases lasting several years (for instance, when investigating the flow of the sea ice sheet in the entire Arctic Ocean region), the prevailing approach is to treat the ice as a plastic material. This is loosely based on qualitative observational evidence that the large-scale floating ice flow patterns resemble those observed in the flows of granular media, for which the application of plasticity theories is the common practice. An example is the viscous-plastic theory developed by Hibler (1979), which, with some modifications, has been applied, more or less successfully, to many problems involving large ice packs in polar regions. Typically, in these problems the main objective has been to determine horizontal displacements of ice; the evaluation of stresses in the ice cover has not been addressed as being unimportant in geophysical applications. In the case of events that last up to several days – and these are the events which are of prime importance to engineering practice, it is much more difficult than in the short- or long-time problems mentioned above to discriminate between the relative significance of different modes of deformation possible to occur in the ice. Hence, a variety of theories have been applied so far to model the behaviour of ice in engineering applications, depending on characteristic strain, strain-rate, and stress levels occurring in problems considered. Most often, though, the viscous, elastic-plastic, or viscous-plastic rheologies have been adopted. In this work we focus on the viscous-plastic rheological model for ice, applying it to a quasi-static problem of

interaction between an ice field and a vertical cylindrical structure, with the main objective to evaluate the forces exerted by the ice on the structure wall.

It is assumed here that the ice field, driven towards the structure by wind-induced drag stresses, is coherent enough to be treated as a continuous sheet expanding in the horizontal plane, rather than a multitude of individual floes of varying dimensions and shapes and interacting with each other in an irregular manner (this assumption, referring to granular media again, is analogous to treating the latter as a continuum rather than an aggregate composed of individual particles). For simplicity, it is supposed that the ice cover has a uniform thickness. Similar problems, involving the interaction of ice with a cylindrical structure, have already been investigated in a number of papers: Wang, Ralston (1983) treated the ice as an elastoplastic material, Sjölind (1985) adopted the viscoelastic ice rheology, and Staroszczyk (2005) solved the problem by employing a non-linearly viscous constitutive law for ice. In the present study the behaviour of ice is modelled by a viscous-plastic flow law with an elliptic yield curve in the two-dimensional principal stress space. Depending on the magnitude of some strain-rate invariant (a combination of the dilatation-rate and the shear-rate in ice), the law predicts either plastic flow (yield) when the former invariant exceeds some critical strain-rate level, or linearly viscous flow when the invariant value is below the critical strain-rate level. The elliptic yield curve is chosen in such a way that the maximum pressure in ice is by about two orders of magnitude larger than the maximum tensile isotropic stress, reflecting the observation that the strength of ice in diverging flow (that is, under tensile stresses) is, due to the development of cracks in ice, significantly smaller than the compressive strength of the material.

In the analysis, the ice sheet equilibrium equations are solved by applying a finite difference method. The results of numerical simulations carried out for a range of parameters defining the strength of ice and the critical strain-rate level defining the onset of ice yield, illustrate the distribution of the forces which the floating ice exerts on the cylinder wall. Two types of boundary conditions at the ice – structure interface, free-slip and no-slip, are considered. The numerical analysis is complemented by comparing the results obtained for the viscous-plastic rheology with those calculated by using the non-linearly viscous flow law (Staroszczyk 2005).

2. Problem Formulation

The floating ice sheet is subject, in general, to the combined action of in-plane and transverse loads. The in-plane loads act tangentially to the ice top and bottom surfaces and are caused by the wind and water drag forces, and the transverse load comes from the vertical reaction of the underlying water. As a result, the ice cover undergoes both axial and shear deformation in the horizontal plane, and bending and twisting that deforms the ice off its middle surface. As we are here

primarily focused on the determination of horizontal forces that are exerted by the ice cover on an engineering object, we neglect in the analysis the bending and twisting effects and restrict attention solely to the analysis of the in-plane axial and shear forces in the ice. Such a simplification is motivated by the fact that the ice sheet off-plane deformations have a very limited effect on the magnitudes of the horizontal forces sustained by the ice, hence their influence on the loads passed from the ice onto the structure may be regarded as insignificant. On the other hand, the ice sheet bending and twisting mechanisms lead to the sheet buckling and its subsequent flexural failure (resulting ultimately in the ice ridging and piling-up), therefore the off-plane modes of deformation affect the maximum axial forces that can develop in the ice sheet, hence they determine, indirectly, the in-plane strength of the floating ice sheet.

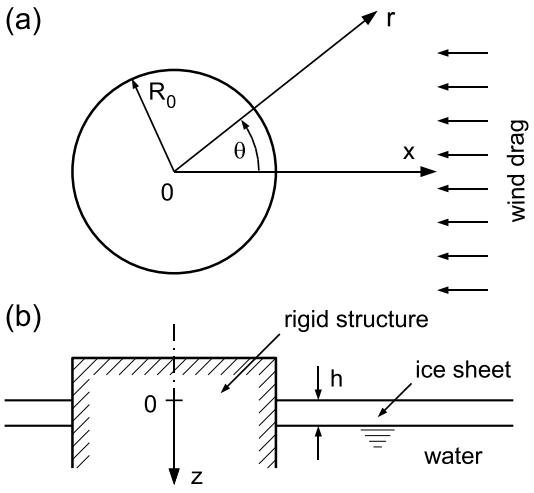

Fig. 1. Geometry of the problem and the adopted polar coordinates: (a) plane view, (b) ice sheet cross-section

Since we are concerned with the problem involving a structure of the circular cross-section in the horizontal plane, we adopt cylindrical polar coordinates r, θ, z $(0 \leq \theta < 2\pi)$, with the vertical z-axis coinciding with the axis of symmetry of the cylinder, as shown in Fig. 1. For simplicity, the region of the ice cover which immediately interacts with the structure is assumed to be of a constant thickness, denoted by h. The ice is assumed to be homogeneous across its depth, that is, the effects of such phenomena as temperature and ice porosity variation with z are neglected. A circular cylinder, of a radius R_0, is treated as a fixed rigid body that interacts with the ice sheet along its vertical walls at $r = R_0$. The purpose of the analysis is to evaluate the horizontal forces which the floating ice exerts on the

cylinder during an interaction event, when a large ice field is pushed towards the structure by the drag stresses generated by wind and/or water currents.

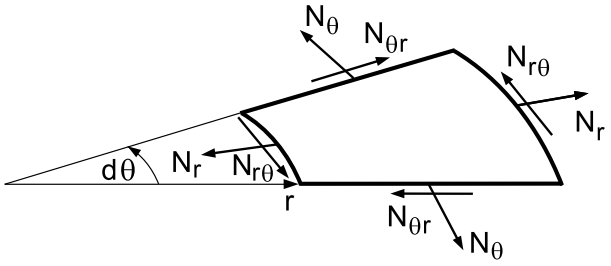

Fig. 2. Definitions of internal axial and shear forces acting on an ice sheet element

Internal in-plane forces acting on an infinitesimal ice sheet element, with components expressed in the adopted polar coordinates, are defined in Fig. 2. The axial forces are denoted by N_r and N_θ, and the shear forces are $N_{r\theta} = N_{\theta r}$, all are measured per unit length along the ice sheet span. The external forces acting in the horizontal direction are those coming from the wind and water drag; their components are denoted by q_r and q_θ. Then, in the absence of inertia forces which are neglected due to small time variations in the ice velocities occurring in natural conditions, the ice equilibrium equations are given by

$$\begin{aligned} &\frac{\partial (r N_r)}{\partial r} - N_\theta + \frac{\partial N_{\theta r}}{\partial \theta} + r q_r = 0, \\ &\frac{1}{r}\frac{\partial (r^2 N_{r\theta})}{\partial r} + \frac{\partial N_\theta}{\partial \theta} + r q_\theta = 0. \end{aligned} \tag{1}$$

The forces driving the ice pack, with the component intensities q_r and q_θ, are adopted in the form of the following quadratic relations

$$\boldsymbol{\tau}_a = C_a \varrho_a (\mathbf{u}_a - \mathbf{v})|\mathbf{u}_a - \mathbf{v}|, \qquad \boldsymbol{\tau}_w = C_w \varrho_w (\mathbf{u}_w - \mathbf{v})|\mathbf{u}_w - \mathbf{v}|, \tag{2}$$

where $\boldsymbol{\tau}_a$ and $\boldsymbol{\tau}_w$ are the tractions due to wind stress and water drag, respectively. The parameters C_a and C_w in the above equations are the dimensionless wind and water drag coefficients (Sanderson 1988), ϱ_a and ϱ_w denote the air and water densities, $\mathbf{u}_a$ and $\mathbf{u}_w$ are the velocity vectors of wind and water current, and $\mathbf{v}$ is the vector of the horizontal velocity of ice. The component loads q_r and q_θ entering Eq. (1) are equal to the sums of the projections of $\boldsymbol{\tau}_a$ and $\boldsymbol{\tau}_w$ on the respective directions r and θ.

The internal forces N_r, N_θ and $N_{r\theta}$ are determined by the depth integration of the axial, σ_{rr} and $\sigma_{\theta\theta}$, and shear, $\sigma_{r\theta}$, stresses. Accordingly, they are expressed by the equations

$$N_r = \int_0^h \sigma_{rr}\,\mathrm{d}z, \quad N_\theta = \int_0^h \sigma_{\theta\theta}\,\mathrm{d}z, \quad N_{r\theta} = \int_0^h \sigma_{r\theta}\,\mathrm{d}z. \tag{3}$$

The stress components in Eq. (3), required to determine the internal forces and hence to solve the equilibrium equations Eq. (1), are related to ice deformations through constitutive laws. As we are concerned only with the viscous-plastic behaviour of the material, neglecting thus any elastic or viscoelastic effects, we adopt constitutive laws which express the stress solely in terms of current strain-rate (that is, no history of deformation is taken into account). Accordingly, we define the two-dimensional strain-rate components D_{rr}, $D_{\theta\theta}$, $D_{r\theta}$ in terms of the components v_r and v_θ of the velocity field $\mathbf{v}$:

$$D_{rr} = \frac{\partial v_r}{\partial r}, \quad D_{\theta\theta} = \frac{1}{r}\left(v_r + \frac{\partial v_\theta}{\partial \theta}\right), \quad D_{r\theta} = \frac{1}{2}\left[\frac{1}{r}\frac{\partial v_r}{\partial \theta} + r\frac{\partial}{\partial r}\left(\frac{v_\theta}{r}\right)\right]. \tag{4}$$

A specific form of the constitutive law adopted to describe the viscous-plastic rheology of ice is discussed in the following section.

3. Viscous-Plastic Rheology of Floating Ice

In typical sea ice – engineering structure events, both reversible (elastic or viscoelastic) and irreversible (plastic) phenomena occur. Therefore, in the first attempts to describe the sea ice rheology, elastic-plastic constitutive models were formulated; an example of these early developments is the paper by Pritchard (1975). However, it was soon realized that during the ice deformations taking place over time scales of the orders imposed by wind forcing (hours and days), the reversible strains become negligibly small compared to irreversible ones. Hence, in subsequent theories constructed to model the sea ice rheology, the elastic behaviour was ignored, giving rise to viscous-plastic formulations. In this way the mathematical and numerical complexities of the models are considerably reduced, since the necessity of keeping track of elastic strains indefinitely (which usually forces a Lagrangian formulation) in a given solution domain is avoided. Such an approach, based on the exclusion of elastic effects in ice, had prevailed for about two decades, until the paper by Hunke and Dukowicz (1997) was published. The authors discovered that the presence of elasticity terms in the equations for ice leads to significant improvement of numerical stability of the model. The enhanced model gives more accurate results for transient states in ice, and reduces to earlier viscous-plastic theories for longer time scales. This modified approach, however, has a drawback as well, since the elastic-like behaviour is not intended to be physically realistic – the specific values of elastic parameters are chosen in such a way that the numerical efficiency of the model is optimized. Hence, these parameters have an artificial character.

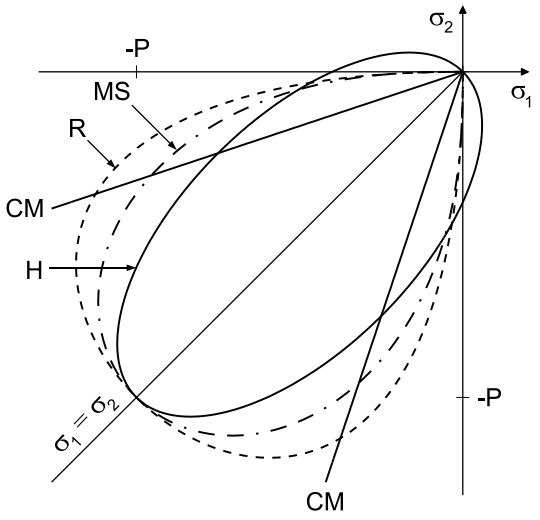

Fig. 3. Comparison of different yield curves for viscous-plastic rheology: H – elliptic curve by Hibler (1979), R – teardrop curve by Rothrock (1975), MS – teardrop curve by Morland and Staroszczyk (1998), CM – Coulomb-Mohr straight lines

We pursue an approach in which the sea ice is consistently treated as a viscous-plastic material. Accordingly, only irreversible deformations are taken into account, that is, no elastic, nor viscoelastic effects are included in the analysis. Therefore, the model cannot be applied to simulate the behaviour of ice over very short time scales, when the irreversible and reversible strains in the material are of comparable magnitudes. It is assumed in the model that two distinct types of deformation in ice occur, depending on the value of a certain critical strain-rate invariant. At strain-rates above the critical level the ice deforms by plastic flow (yield), whereas below that critical strain-rate the ice is supposed to deform by viscous flow. The limit stress level in the ice during its plastic flow is defined by a yield curve, the shape of which prescribes admissible stress states in the medium, for instance the magnitudes of maximum shear stresses compared to the axial stresses. Different shapes of the yield curves for sea ice have been proposed and investigated numerically so far; some of them, plotted in principal stress axes (σ_1, σ_2), with positive values denoting tension, are presented in Fig. 3. In the first viscous-plastic model for ice, originally formulated by Hibler (1977, 1979), and further improved by Ip et al (1991) and Hibler and Ip (1995), an elliptic yield curve was adopted (the solid line in the figure). Rothrock (1975) proposed, by considering the energetics of plastic flow of ice during its ridging, a teardrop yield curve (the dashed line); the latter, though, has not been implemented in numerical sea ice models. A stress envelope of the shape similar to the Rothrock curve was proposed, and investigated in sea ice flow simulations, by Morland and Staroszczyk (1998), the dashed-dotted line; the latter authors, however, used it to bound stresses in

their non-linearly viscous model, an alternative to the viscous-plastic rheology. For comparison, the yield curve for the classical Coulomb-Mohr rheology, widely applied for granular media, is also shown in Fig. 3 (the solid straight lines). Some other shapes of the yield curves, not depicted in the figure, have also been explored. These include a straight line for a so-called cavitating fluid (a fluid with no shear resistance, Flato, Hibler 1992), square yield curve (Ip et al 1991), and 'ice-cream-cone' curve (Tremblay, Mysak 1997, Tremblay 1999). Comparison analyses for different sea ice viscous-plastic models have been carried out by Ip et al (1991), Schulkes et al (1998), and Tremblay (1999). The results have shown that there are significant similarities between the models including the elliptic and square yield curves, and between the cavitating fluid and Coulomb-Mohr models (Ip et al 1991). Comparisons between numerically predicted and observed sea ice drift data performed for the models implementing the elliptic yield curve and the cavitating fluid rheology seem to give advantage to the former (Tremblay 1999).

All the yield curves shown in Fig. 3, except the Coulomb-Mohr straight lines, characterize the ice of the compressive strength equal to P, and the tensile strength equal to zero. The latter feature, with no resistance of ice to isotropic tensile stresses (occurring in diverging flow), is a source of serious problems encountered in numerical simulations. Namely, it has always been found in the computational models for sea ice that setting stress to be identically zero in diverging flow gives rise to numerical instabilities and subsequent breakdown of the flow simulation, since an arbitrarily small change in the divergence rate through zero results in a large change in the response of the system. Therefore, artificial terms are usually added to the sea ice flow problems governing equations in order to render numerical schemes stable. Commonly, diffusive terms are added (Hibler 1979, Ip et al 1991, Tremblay, Mysak 1997), which introduce some fictitious damping into the problems considered. This must result in the appearance of some unphysical features in the solutions obtained (Gray and Killworth 1995), but it is believed that such artificial effects do not distort significantly the results of simulations. Another method, applied by Schulkes et al (1998) and Morland and Staroszczyk (1998), consists in allowing the stresses to change continuously during a transition from converging to diverging flow regime, so that some small tensile stresses are permitted in the ice. Such a smooth variation in stress, occurring within a narrow range of positive dilatation rates, improves considerably the stability of numerical models for floating ice, although does not guarantee an unconditional stability of numerical algorithms.

In the present work we pursue another approach. We apply an elliptic yield curve, analogous to that proposed by Hibler, but instead of zero tensile strength, we allow a small strength of ice in diverging flow. Hence, we define two strength parameters: $P_1 > 0$ for compression and $P_2 > 0$ for tension, with $P_1 \gg P_2$. In this manner, without introducing artificial diffusion terms in the flow equations, we hope to improve the stability of a numerical method, but still preserve in the

model an important physical feature of very small tensile strength of ice compared to its compressive strength. The adopted yield curve, plotted in two-dimensional principal stress space, is illustrated in Fig. 4 (the solid line).

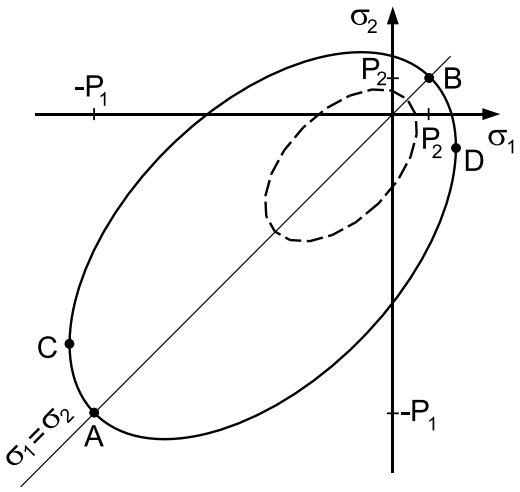

Fig. 4. Elliptic yield curve (solid line) with the ice compressive strength P_1 (stress point A) and small tensile strength P_2 (point B), and a smaller ellipse (dashed line) describing stress states during viscous flow

The elliptical yield curve presented in Fig. 4 is specified by the equation

$$F(\sigma_1, \sigma_2) = (\sigma_1 + \sigma_2 + P_1 - P_2)^2 + e^2 (\sigma_1 - \sigma_2)^2 - (P_1 + P_2)^2 = 0, \qquad (5)$$

where σ_1 and σ_2 are the principal stress components, and e is the ellipse eccentricity (the ratio of the major to the minor axis lengths of the ellipse). In physical terms, e defines the ratio of the maximum shear yield stress in the material to the maximum yield mean pressure: the smaller value of the latter parameter, the smaller is the shear resistance of ice.

Following Hibler (1977), we assume that the material during its yield (when the stress lies on the yield curve) obeys a normal flow rule, implying that the principal strain-rate vector is normal to the yield curve $F(\sigma_1, \sigma_2)$. Hence, we apply the associated flow law expressed by

$$D_{ij} = \lambda \frac{\partial F(\sigma_{ij})}{\partial \sigma_{ij}} \bigg|_{F=0}, \quad i, j = 1, 2, \quad \lambda > 0, \qquad (6)$$

where λ is a function of strain-rate. Adopting the orthogonal coordinate axes x_1 and x_2 to coincide with the principal stress axes, the axial strain-rate components given by Eq. (6) are

$$D_{11} = 2\lambda\left[\sigma_{11}(1+e^2) + \sigma_{22}(1-e^2) + P_1 - P_2\right],$$
$$D_{22} = 2\lambda\left[\sigma_{11}(1-e^2) + \sigma_{22}(1+e^2) + P_1 - P_2\right], \tag{7}$$

with $D_{12} = 0$ on the yield curve. Equations (7) give the axial stress components expressed in terms of the strain-rate components by

$$\sigma_{11} = \frac{1}{8\lambda e^2}\left[2D_{11} + (e^2-1)(D_{11}+D_{22}\right] - \frac{1}{2}(P_1 - P_2),$$
$$\sigma_{22} = \frac{1}{8\lambda e^2}\left[2D_{22} + (e^2-1)(D_{11}+D_{22}\right] - \frac{1}{2}(P_1 - P_2). \tag{8}$$

The above stresses, inserted into Eq. (5), determine the function λ as

$$\lambda = \frac{\Delta}{4(P_1+P_2)}. \tag{9}$$

In Eq. (9), Δ is a strain-rate invariant given by

$$\Delta^2 = \eta^2 + 4\gamma^2/e^2, \tag{10}$$

and is a function of two other strain-rate invariants, namely the dilatation-rate η and the shear-rate γ, defined by

$$\eta = \text{tr } \mathbf{D}, \quad \gamma^2 = \tfrac{1}{2}\text{tr } \hat{\mathbf{D}}^2, \tag{11}$$

where $\mathbf{D}$ is the strain-rate tensor and $\hat{\mathbf{D}}$ is its deviatoric part expressed by

$$\hat{\mathbf{D}} = \mathbf{D} - \tfrac{1}{2}\eta\mathbf{I}, \tag{12}$$

with $\mathbf{I}$ denoting the unit tensor. In terms of the principal strain-rates D_{11} and D_{22}, the two latter invariants are given by

$$\eta = D_{11} + D_{22}, \quad \gamma^2 = \tfrac{1}{4}\,(D_{11} - D_{22})^2, \tag{13}$$

while in arbitrary polar coordinates (with r and θ not necessarily aligned with the principal stress/strain-rate directions at a point), they become

$$\eta = D_{rr} + D_{\theta\theta}, \quad \gamma^2 = D_{r\theta}^2 + \tfrac{1}{4}\,(D_{rr} - D_{\theta\theta})^2, \tag{14}$$

with the strain-rate components defined by Eq. (4).

Substitution of the definition (9) into equations (8) eliminates the function λ from the latter, so that the stresses are expressed in terms of the strain-rate components and their invariants, as well as the coefficients P_1, P_2 and e defining the shape of the yield curve. By introducing the parameters

$$\zeta = \frac{P_1+P_2}{2\Delta}, \quad \mu = \frac{\zeta}{e^2} = \frac{P_1+P_2}{2\Delta e^2}, \tag{15}$$

the stresses in ice can be described by the following tensor relation

$$\boldsymbol{\sigma} = 2\mu\mathbf{D} + \left[(\zeta - \mu)\eta - \frac{1}{2}(P_1 - P_2)\right]\mathbf{I}, \tag{16}$$

which expresses the plastic flow law for ice in the frame-indifferent form. By comparing Eq. (16) with the Reiner-Rivlin form of the constitutive law for a non-linearly viscous fluid (Chadwick 1999), we note that ζ and μ can be identified as the bulk and shear viscosities of ice, respectively, both being functions of the ice strength parameters P_1 and P_2 and the strain-rate invariant Δ. It can be readily verified that in the particular case of purely converging or diverging flow, when $\sigma_{11} = \sigma_{22}$ (so that the stress points lie on the straight line $\sigma_1 = \sigma_2$ in Fig. 4), the flow law given by Eq. (16) reduces to

$$p = -\frac{1}{2}\left[(P_1 + P_2)\mathrm{sgn}(\eta) - (P_1 - P_2)\right], \tag{17}$$

where $p = -(\sigma_{11} + \sigma_{22})/2$ is the mean pressure. In converging flow (ice compression, $\eta < 0$ and $\mathrm{sgn}(\eta) = -1$), the latter relation gives $p = P_1$, or $\sigma_{11} = \sigma_{22} = -P_1$, while in diverging flow (ice extension, $\eta > 0$ and $\mathrm{sgn}(\eta) = +1$), equation (17) supplies $p = -P_2$, or $\sigma_{11} = \sigma_{22} = P_2$. Hence, the predicted responses coincide with the stress points A and B in Fig. 4, as expected.

The flow law (16), in conjunction with the viscosity definitions (15), describes the behaviour of ice at yield. The latter is assumed to occur when the strain-rate invariant Δ reaches a certain critical level, denoted by Δ_c, that is, plastic deformations take place when $\Delta \geq \Delta_c$. Below that critical level, when $\Delta < \Delta_c$, ice is supposed to undergo viscous deformations, with constant (independent of the current strain-rate) viscosities. These are set to be equal to the viscosities at the onset of yield (Hibler 1979), that is, when $\Delta = \Delta_c$. Hence, in view of Eq. (15), they are defined by

$$\zeta_m = \frac{P_1 + P_2}{2\Delta_c}, \quad \mu_m = \frac{P_1 + P_2}{2\Delta_c e^2}. \tag{18}$$

The latter are the upper bounds for the bulk and shear viscosities of the medium, and occur at the values of the deformation-rates for which Δ does not exceed the critical level Δ_c. At higher strain-rates, when $\Delta > \Delta_c$, the ice viscosities decrease monotonically to zero with increasing Δ, as prescribed by the definitions (15), albeit the stresses remain on the yield curve as Δ grows indefinitely. In the original formulation by Hibler (1979), for $\Delta < \Delta_c$, stresses predicted by the flow law lie on a family of smaller ellipses that are concentric with the yield ellipse, and their both axes decrease as Δ decreases, vanishing at $\Delta = 0$. This leads to a physically unsound response in which isotropic stress arises in ice in the absence of any deformation. This disadvantage of the constitutive model was subsequently avoided by Hibler and Ip (1995), who proposed the dependence of the pressure

term in their flow law (analogous to the term $(P_1 - P_2)$ in Eq. (16)) on the current strain-rate. We make use of the same idea, that is, for $\Delta < \Delta_c$, scale down the pressure coefficients P_1 and P_2 by a factor Δ/Δ_c :

$$P_1 \to \frac{\Delta}{\Delta_c} P_1, \quad P_2 \to \frac{\Delta}{\Delta_c} P_2, \quad \Delta < \Delta_c \, .$$

Thus, there are two distinct relations describing the behaviour of ice. One that describes plastic yield for $\Delta \geq \Delta_c$, given by Eq. (16), and one that describes viscous flow for $\Delta < \Delta_c$. These are combined into the following form of the constitutive law:

$$\boldsymbol{\sigma} = \begin{cases} 2\mu \mathbf{D} + \left[(\zeta - \mu)\eta - \dfrac{1}{2}(P_1 - P_2) \right] \mathbf{I} & \text{if} \quad \Delta \geq \Delta_c \, , \\ 2\mu_m \mathbf{D} + \left[(\zeta_m - \mu_m)\eta - \dfrac{\Delta}{2\Delta_c}(P_1 - P_2) \right] \mathbf{I} & \text{if} \quad \Delta < \Delta_c \, , \end{cases} \tag{19}$$

with the viscosities ζ and μ, and ζ_m and μ_m, defined by Eq. (15) and Eq. (18), respectively. It can be shown that, for $\Delta < \Delta_c$, the stresses predicted by Eq. (19_2) lie on an ellipse whose centre approaches the stress origin and the major and minor axes decrease monotonically to zero as $\Delta \to 0$. One such an ellipse is plotted in Fig. 4 (the dashed line).

The constitutive model given by Eq. (19) has four free parameters: P_1 and P_2 defining, respectively, compressive and tensile strength of ice, Δ_c prescribing the critical strain-rate at which plastic yield starts, and e defining, through Eq. (15) and Eq. (18), the ratio of the shear to axial viscosities of ice.

4. Numerical Results and Discussion

Combination of the two equilibrium equations (1) with the internal forces definitions (3), the constitutive relations (19), and the strain-rates expressions (4), transforms the problem formulated in Section 2 to the solution of two partial differential equations for the two unknown horizontal velocity fields, v_r and v_θ. The latter two equations have been solved numerically by a finite difference method, in which all partial derivatives have been approximated by standard central differences. Owing to the symmetry of the problem with respect to the wind direction which is assumed to blow along the coordinate line $\theta = 0$, only the region $0 \leq \theta \leq \pi$ has been considered in the numerical model. In the radial direction, the ice domain extends from the cylinder wall at $r = R_0$ to the free edge of the ice cover at $r = R_{\max}$. The adopted computational mesh has 300 nodes in the radial direction and 61 nodes in the circumferential direction, uniformly distributed along both r and θ, so that there are 18300 nodes in all, with 36600 unknown values of the velocities to be calculated. At the ice – structure contact surface

either no-slip (full bonding) or free-slip boundary conditions are assumed for the ice deformation. For a no-slip boundary these are expressed by

$$r = R_0 : \quad \mathbf{v} = \mathbf{0}, \tag{20}$$

whereas for a free-slip boundary they are defined by

$$r = R_0 : \quad \mathbf{v} \cdot \mathbf{n} = 0, \quad N_{r\theta} = 0, \tag{21}$$

where $\mathbf{n}$ is the unit vector normal to the cylinder wall. The ice at the outer edge $r = R_{\max}$ is assumed to be stress-free, that is,

$$r = R_{\max} : \quad N_r = 0, \quad N_{r\theta} = 0. \tag{22}$$

Simulations have been carried out for a cylinder of the radius $R_0 = 10$ m, situated at the centre of a circular ice field extending to $R_{\max} = 500$ m, with the thickness of the ice cover equal to $h = 0.2$ m. The ice is assumed to be driven onto the structure by wind of a constant velocity $u_a = 20\ \mathrm{m\,s^{-1}}$, blowing along the coordinate line $\theta = 0$ in the negative direction of r. Hence, we neglect transient states in the ice occurring for smaller wind velocities, that is before the wind reaches the above limit value u_a. In other words, we neglect the history of loading leading up to that limit situation, and consider only a "steady" viscous-plastic flow during which, in view of the rheological model adopted, the magnitudes of forces acting on the structure attain their extremal values. The dimensionless atmospheric drag coefficient, appearing in Eq. (2), is assumed to have the value $C_a = 2 \times 10^{-3}$ (Sanderson 1988), and the air density is $\varrho_a = 1.3\ \mathrm{kg\,m^{-3}}$. For simplicity, drag forces due to water currents are neglected.

The viscous-plastic behaviour of ice predicted by the constitutive laws (19) is determined by the particular values of the four constitutive parameters: P_1, P_2, e and Δ_c, from among which the first and the last, P_1 and Δ_c, are most important in terms of quantitative results. Regarding the compressive strength of ice, P_1, there is no clarity in the literature as to its most proper magnitude. In the original viscous-plastic model, Hibler (1979) used the value 5×10^3 Pa for large-scale Arctic ice simulations, and the latter value was subsequently used by him and co-authors in a number of papers (Ip et al 1991, Hibler, Ip 1995). Flato and Hibler (1992), in turn, applied a larger value, 2.75×10^4 Pa, again for describing the large-scale behaviour of ice. In our simulations, we have adopted the value $P_1 = 5 \times 10^4$ Pa, slightly larger than the latter, based on the belief that the ice strength increases with decreasing spatial scale of the problem involved (Sanderson 1988). The adopted magnitude of P_1 ensures that the domain of ice in which plastic flow occurs spreads out from the structure wall to the distance of several radii of the cylinder. This follows from the results obtained by Staroszczyk (2005), who investigated the problem with the same ice field geometry as the

present, but with a viscous fluid rheology of ice. Also based on the results presented in the latter paper, we have adopted for the critical strain-rate invariant the value $\Delta_c = 2 \times 10^{-5}$ s^{-1}, which can be treated as a typical strain-rate magnitude occurring in the vicinity of the structure under the assumed ice and wind conditions. The rheological model parameter e, defining the shape of the yield curve, and hence the magnitude of the shear viscosity relative to the bulk viscosity, was commonly assumed (Hibler 1979) as 2 (that is, $\mu/\zeta = 1/4$). In our simulations we have explored the range $1 \leq e \leq 3$. The remaining constitutive model parameter, P_2, used in the present formulation to define the tensile strength of ice, has been adopted as a small fraction of the compressive strength P_1. Accordingly, we have adopted $P_2 = 1 \times 10^3$ Pa, that is, $P_2 = P_1/50$. Smaller values of P_2 have been tried, but they led to numerical instabilities for $e \gtrsim 2$ (and we recall that the primary purpose of introducing $P_2 > 0$ into our model has been to avoid instabilities encountered in previous viscous-plastic models). Although it is likely that a smaller value of P_2 would better reflect the physics of sea ice, the results of simulations have shown that the specific magnitude of this parameter does not have much effect on total horizontal forces sustained by an engineering object, since most of the loading comes from the ice that is under compression on the windward side of the structure.

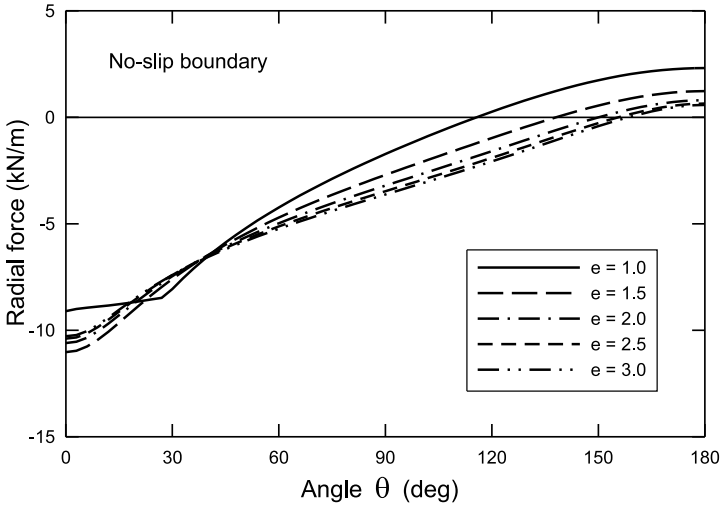

Fig. 5. Distribution of the radial forces N_r along the cylinder wall for no-slip boundary conditions and different values of the rheological parameter e

Figs. 5 and 6 present the distribution of the forces exerted by the ice on the structure wall in the case of no-slip boundary conditions. Shown is the dependence of the contact forces on the rheological parameter e, that is, the effect of the ratio of the shear to bulk viscosities of ice is demonstrated. The range of e from 1 to 3 corresponds to the viscosity ratios μ/ζ (or μ_m/ζ_m) decreasing from 1 (for

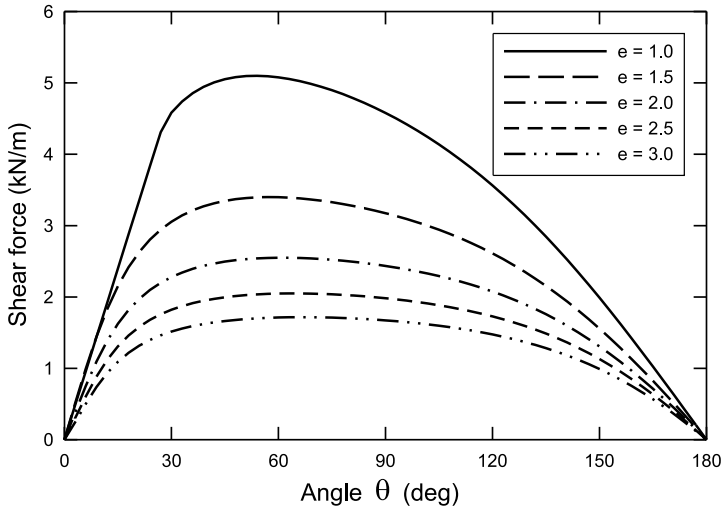

Fig. 6. Distribution of the shear forces $N_{r\theta}$ along the cylinder wall for no-slip boundary conditions and different values of the rheological parameter e

$e = 1$) to $1/9 \sim 0.111$ (for $e = 3$), with the bulk viscosity ζ held constant for a given strain-rate invariant Δ, as prescribed by equation (15). Fig. 5 illustrates the variation of the radial force N_r with the polar angle θ. We observe that the effect of the shear viscosity on the magnitude of N_r, for the no-slip boundary, is moderate, particularly on the windward side of the structure. For the chosen ice and wind parameters, the ice at the cylinder wall is in plastic flow for all e and θ, except for the case of $e = 1$ (the solid line) when, for $\theta \lesssim 30^\circ$, viscous deformation occurs – this feature will be further illustrated in Fig. 8. Comparing the magnitudes of the maximum tensile forces at $\theta = 180^\circ$ and compressive forces at $\theta = 0$, we see that their ratio is much greater (especially for smaller e) than the strength parameters ratio, $P_2/P_1 = 1/50$. This may appear surprising, but can be explained by referring to Fig. 4, showing the elliptic yield curve. Assuming that $\sigma_1 = \sigma_{rr}$ and $\sigma_2 = \sigma_{\theta\theta}$, the stress state in the ice at the wall at $\theta = 0$ (converging flow) corresponds to the stress point C on the ellipse, while the stress state at $\theta = 180^\circ$ (diverging flow) corresponds to the point D on the yield curve. For small values of the ellipse eccentricity parameter e (the case $e = 1$ corresponds to a circle), the tensile stress $\sigma_1 = \sigma_{rr}$ at the point D can be much greater than P_2. This feature, of tensile stresses significantly exceeding the tensile strength parameter P_2, is an obvious consequence of the adopted shape of the yield curve.

The distribution of the shear forces $N_{r\theta}$ along the cylinder wall is shown in Fig. 6. We note that the shear forces exerted by the floating ice change smoothly with the angle θ, with maximum values occurring at $\theta \sim 60^\circ$. Hence, the magnitudes of $N_{r\theta}$ on the windward side of the structure are larger than those on the

leeward side, though the differences are not considerable, especially for smaller values of the shear viscosity.

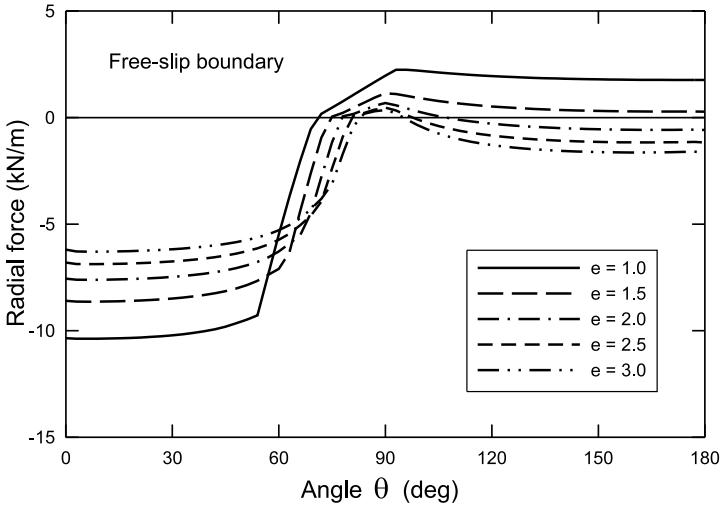

Fig. 7. Distribution of the radial forces N_r along the cylinder wall for free-slip boundary conditions and different values of the rheological parameter e

Fig. 7 illustrates the variation of the normal forces N_r with the angle θ and the rheological parameter e in the case of a free-slip boundary, when the tangential forces $N_{r\theta}$ are identically zero. Comparing this figure with the analogous plots in Fig. 5 for no-slip boundary conditions, we immediately note qualitatively distinct distributions of radial forces along the cylinder wall. While in the no-slip case the forces N_r vary in a monotonic way over the entire range of θ, dramatic changes in the values of N_r are predicted by the rheological model for the free-slip boundary. These changes occur within the range $60^\circ \lesssim \theta \lesssim 90^\circ$, where the normal forces switch rapidly from compressive to tensile ones, with the maximum tensile forces occurring at $\theta \sim 90^\circ$. As the results displayed below in Fig. 9 show, within the latter range of θ the ice is in viscous flow, in contrast to the rest of the wall where it deforms plastically. Another feature worth noting is that for $e \gtrsim 1.5$, that is for the viscosity ratios $\mu/\zeta \lesssim 0.4$, compressive forces can occur not only on the windward, but also on the leeward side of the cylinder.

Corresponding to the above plots of the normal and shear contact forces are Figs. 8 and 9 showing the variation of the strain-rate invariant Δ with the angle θ for different values of e. The latter invariant is normalized by the magnitude of the critical strain-rate invariant Δ_c; that is, the ratios Δ/Δ_c are plotted in the figures. Since Δ_c defines the strain-rate level at which plastic yield starts, the values of $\Delta/\Delta_c < 1$ indicate that the ice deforms as a viscous material, whereas for $\Delta/\Delta_c \geq 1$ plastic flow occurs at given points on the cylinder wall. Fig. 8 illustrates the distribution of Δ/Δ_c for a no-slip boundary. It is seen that, for $e \geq 1.5$, the ice

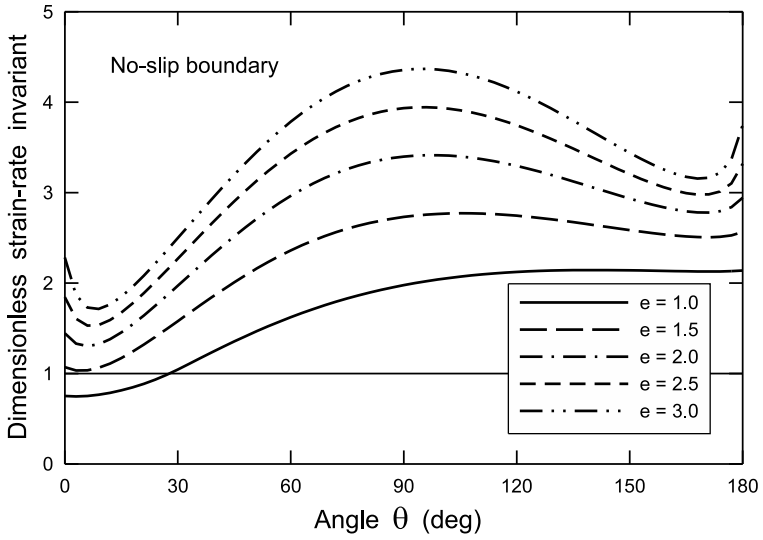

Fig. 8. Variation of the dimensionless strain-rate invariant Δ/Δ_c along the cylinder wall for no-slip boundary conditions and different values of the rheological parameter e

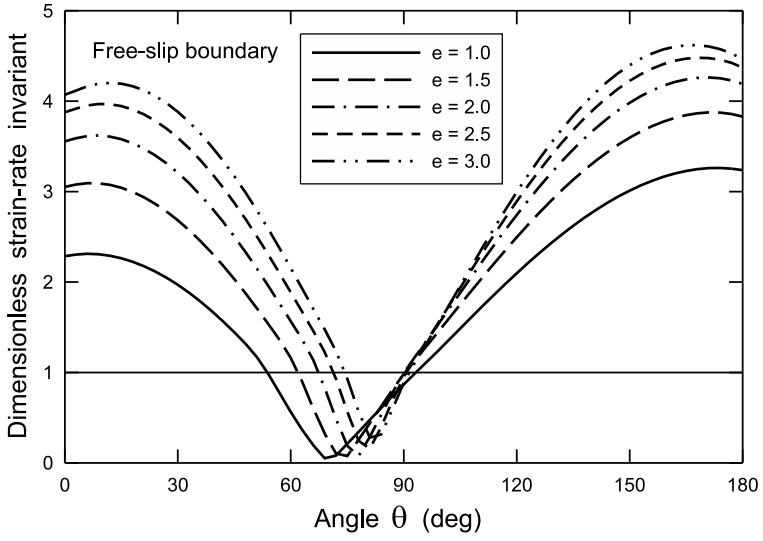

Fig. 9. Variation of the dimensionless strain-rate invariant Δ/Δ_c along the cylinder wall for free-slip boundary conditions and different values of the rheological parameter e

deforms plastically along the whole structure wall, and only in the case of $e = 1$ (that is, when the shear and bulk viscosities are equal), the critical level of the strain-rate invariant is not reached for $\theta \lesssim 30^\circ$ and, hence, the ice is in viscous flow. We also note that the maximum values of the strain-rate invariant Δ occur at the angles close to 90°. Quite a different situation takes place in the case of a free-slip boundary, as illustrated in Fig. 9, since now the maximum values of Δ occur at the angles $\theta \sim 0^\circ$ and $\theta \sim 180^\circ$. Another characteristic feature observed in Fig. 9 is that, irrespective of the value of the parameter e (that is, of the viscosity ratio μ/ζ), the normalized invariant Δ/Δ_c reaches values close to zero at some (dependent on e) angles θ from within the range $70^\circ \lesssim \theta \lesssim 80^\circ$. Accordingly, the ice in the vicinity of such peculiar points deforms in viscous regime, as opposed to the remaining part of the cylinder wall where it undergoes plastic yield.

Finally, the predictions of the viscous-plastic rheological model have been compared with the results given by the non-linearly viscous model proposed by Staroszczyk (2005). In the latter formulation, it is assumed that the ice viscosities have constant values in converging flow, and decrease very quickly in a narrow range of strain-rates at the start of diverging flow. This significant viscosity reduction, by three to four orders of magnitude, is strongly non-linear in strain-rate and reflects rapid weakening of ice with increasing tensile deformation. In order to compare the predictions of the two rheologies, we adopt in both models the same maximum bulk and shear viscosities, ζ_m and μ_m, as defined by Eq. (18). Thus, with the viscous-plastic model parameters unchanged ($P_1 = 5 \times 10^4$ Pa, $P_2 = 1 \times 10^3$ Pa, $\Delta_c = 2 \times 10^{-5}$ s^{-1}), we set in the viscous model $\zeta = 1.25 \times 10^9$ kg m^{-1} s^{-1}, with $\mu = e^{-2}\zeta$, that is dependent on e. Below, we present the distributions of the contact forces for two values of the parameter e, 1.5 and 2.0. The corresponding shear viscosities μ in the viscous model are then 5.55×10^8 kg m^{-1} s^{-1} and 3.12×10^8 kg m^{-1} s^{-1}, respectively. In the non-linearly viscous model for ice, the critical strain-rate level around which significant changes in ζ and μ occur is defined by the dilatation-rate η_c, which is different from the plastic yield critical strain-rate invariant Δ_c (incorporating both the η and γ invariants) used in the viscous-plastic formulation. To correlate these two different rheological parameters, we assume that, on average, η and γ have comparable contributions to the value of Δ_c, that is, $|\eta| \sim \gamma$. Hence, in view of Eqs. (10) and (13), we have $\eta_c = \Delta_c(1 + 4/e^2)^{-1/2}$, that is, $\eta_c = 1.2 \times 10^{-5}$ s^{-1} for $e = 1.5$, and $\eta_c = 1.41 \times 10^{-5}$ s^{-1} for $e = 2.0$. In Fig. 10 the distributions of the radial forces N_r along the cylinder wall for a no-slip boundary are compared. We note that both rheologies give very similar magnitudes of the extremal, compressive and tensile, contact forces on the wall. Similar is also the overall character of the variations of N_r with θ for both rheological models, with significant differences occurring only within the range of polar angles $90^\circ \lesssim \theta \lesssim 120^\circ$. A different picture is observed in Fig. 11 which illustrates the distributions of the radial forces N_r on

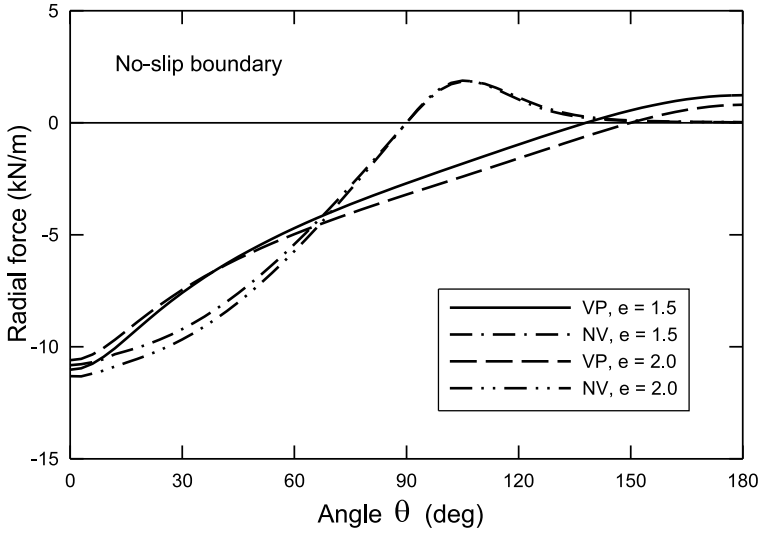

Fig. 10. Distribution of the radial forces N_r along the cylinder wall for no-slip boundary conditions. Compared are the results for the viscous-plastic (VP) and non-linearly viscous (NV) ice rheologies

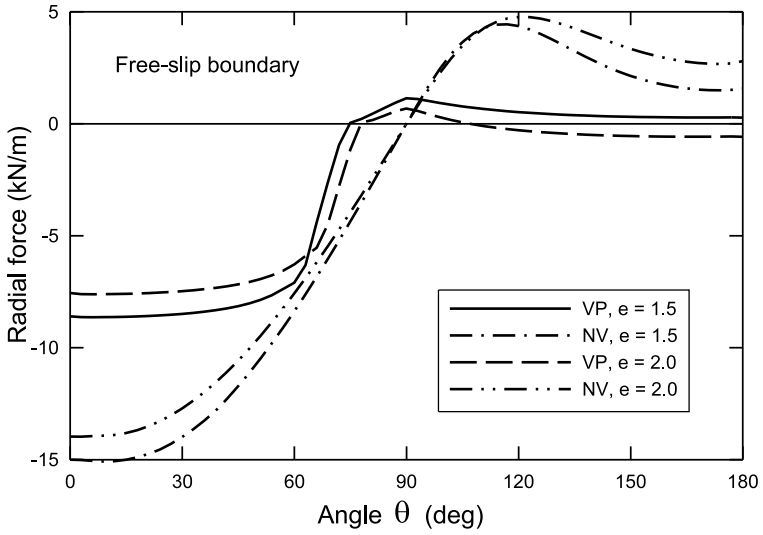

Fig. 11. Distribution of the radial forces N_r along the cylinder wall for free-slip boundary conditions. Compared are the results for the viscous-plastic (VP) and non-linearly viscous (NV) ice rheologies

a free-slip wall. Since in this case the viscous rheology predicts considerably larger (by about 40 per cent) contact forces on the windward side of the wall when compared to no-slip boundary conditions (Staroszczyk 2005), the discrepancies between the predictions of the two rheological models are substantial – mainly in terms of the quantitative results, as still noticeable qualitative similarities can be seen.

5. Concluding Remarks

In the paper we have extended the viscous-plastic rheological model with an elliptic yield curve which is customarily employed in large-scale simulations of the floating ice behaviour. The extension consists in introducing into the model an additional parameter that can be interpreted as the tensile strength of ice in isotropic stress state. The aim of the modification is to avoid artificial diffusion terms that are commonly included into the flow governing equations to ensure the stability of numerical computations, since such terms give rise to unphysical effects in the solutions obtained. The proposed constitutive model has been used to calculate the magnitudes of forces that floating ice exerts on a cylindrical structure, and it has turned out that, indeed, the modified form of the flow law improves the numerical stability, provided that the tensile strength is no less than 1/50 of the compressive strength of the ice. The results of simulations, carried out for no-slip and free-slip conditions at the ice – structure interface, show that the tensile normal forces on the leeward side of the cylinder, where diverging ice flow prevails, may reach the magnitudes that are about 1/5 of the maximum compressive forces on the windward side (see Figs. 5 and 7). The predictions of the viscous-plastic model have also been compared with those given by the non-linear rheology of ice. The results (Figs. 10 and 11) show that relatively good agreement occurs in the case of no-slip boundary conditions at the wall, whereas considerable differences between the predictions of both rheological models take place in the free-slip case. The appearance of significant tensile stresses in the solutions predicted by the viscous-plastic rheology, the feature which is due to the particular shape of the elliptic yield curve, seems to be somewhat unrealistic behaviour of floating ice. It is possible that adopting yield curves which lie entirely in the negative principal stress quadrant would give the predictions which are in better agreement with observations. However, such shapes of the yield curve (at least those sketched in Fig. 3) do not allow the normal flow rule; hence, the formal description of the ice behaviour during yield will be more complex. Moreover, it is anticipated that with other shapes of the yield curve it will be even more difficult to maintain the numerical stability than it is in the case of the elliptic curve adopted in this work.

The analysis presented in the paper demonstrates a general method of calculating the contact forces which a floating ice pack exerts on an engineering structure. The ice has been modelled here as a viscous-plastic material, though,

obviously, the same, or a similar, method applies in the case of other rheologies of ice. However, there is still some way to go before specific engineering problems involving sea ice – structure interactions can be solved with a sufficient degree of confidence. First of all, it is not clear yet which particular constitutive model describes best the real sea ice rheology. In other words, the role, and relative significance, of elastic, viscous and plastic effects in the material behaviour at different strains, strain-rates and stress levels is not properly identified yet. Another important question in the field of sea ice modelling concerns the values of physical parameters describing the material, most notably the strength of ice in compression and extension, and its dependence on the rate of deformation. Particular values scattered in the literature vary considerably, often by more than one order of magnitude, which contributes to uncertainties associated with quantitative predictions of theoretical analyses. The only method of identification of rheological properties of the sea ice, and the validation of theoretical models as well, is by field observations. However, even if these are possible to perform for certain particular engineering problems, it is difficult to generalize the results so obtained because of the vast variety of the sea ice types and weather conditions (i.e. deformation regimes) encountered in practice. That is, the results of physical measurements obtained for one specific ice – structure interaction problem should be transferred to other problems with great caution.

References

Chadwick P. (1999), *Continuum Mechanics: Concise Theory and Problems*, Dover, Mineola, New York, 2nd edn.

Flato G. M. and Hibler W. D. (1992), Modeling pack ice as a cavitating fluid, *J. Phys. Oceanogr.*, Vol. 22 (6), 626–651.

Gray J. M. N. T., Killworth P. D. (1995), Stability of the viscous-plastic sea ice rheology, *J. Phys. Oceanogr.*, Vol. 25, 971–978.

Hibler W. D. (1977), A viscous sea ice law as a stochastic average of plasticity, *J. Geophys. Res.*, Vol. 82 (27), 3932–3938.

Hibler W. D. (1979), A dynamic thermodynamic sea ice model, *J. Phys. Oceanogr.*, Vol. 9 (4), 815–846.

Hibler W. D., Ip C. F. (1995), The effect of sea ice rheology on Arctic buoy drift, *ASME AMD*, Vol. 207, 255–263.

Hunke E. C., Dukowicz J. K. (1997), An elastic-viscous-plastic model for sea ice dynamics, *J. Phys. Oceanogr.*, Vol. 27, 1849–1867.

Ip C. F., Hibler W. D., Flato G. M. (1991), On the effect of rheology on seasonal sea-ice simulations, *Ann. Glaciol.*, Vol. 15, 17–25.

Morland L. W., Staroszczyk R. (1998), A material coordinate treatment of the sea-ice dynamics equations, *Proc. R. Soc. Lond.*, Vol. A 454, 2819–2857.

Pritchard R. S. (1975), An elastic-plastic constitutive law for sea ice, *J. Appl. Mech., Ser. E*, Vol. 42 (2), 379–384.

Rothrock D. A. (1975), The energetics of the plastic deformation of pack ice by ridging, *J. Geophys. Res.*, Vol. 80 (33), 4514–4519.

Sanderson T. J. O. (1988), *Ice Mechanics. Risks to Offshore Structures*, Graham and Trotman, London.

Schulkes R. M. S. M., Morland L. W., Staroszczyk R. (1998), A finite-element treatment of sea ice dynamics for different ice rheologies, *Int. J. Numer. Anal. Meth. Geomech.*, Vol. 22 (3), 153–174.

Sjölind S. G. (1985), Viscoelastic buckling analysis of floating ice sheets, *Cold Reg. Sci. Technol.*, Vol. 11 (3), 241–246.

Staroszczyk R. (2005), Loads exerted by floating ice on a cylindrical structure, *Arch. Hydroeng. Environ. Mech.*, Vol. 52 (1), 39–58.

Tremblay L. B. (1999), A comparison study between two visco-plastic sea-ice models, [in:] *Advances in Cold-Region Thermal Engineering and Sciences* (eds. K. Hutter, Y. Wang and H. Beer), Springer, Berlin, 333–352.

Tremblay L. B., Mysak L. A. (1997), Modeling sea ice as a granular material, including the dilatancy effect, *J. Phys. Oceanogr.*, Vol. 27, 2342–2360.

Wang Y. S. and Ralston T. D. (1983), Elastic-plastic stress and strain distributions in an ice sheet moving against a circular structure, *Proc. Seventh International Conf. on Port and Ocean Engineering under Arctic Conditions, Helsinki 1983*, 940–951.